Journal of Optoelectronic and Biomedical Materials Vol. 12, No. 2, April - June 2019, p. 33 - 42

SYNTHESIS, CHARACTERIZATION, AND ANTIBACTERIAL ACTIVITY OF COBALT DOPED (α-Fe_2O_3) THIN FILMS

D. BEKKAR[a], Y. MEFTAH[a,b], B. BENHAOUA[b,c,*], A. RAHAL[a,b,c],
A. BENHAOUA[a,b,c], A. H. HAMZAOUI[d]
[a]*Faculty of Exact Sciences, University of Echahid Hamma Lakhdar, El Oued 39000, Algeria*
[b]*Lab. VTRS, Faculty of Science & Technology, Univ. El-Oued, El oued 39000, Algeria*
[c]*Unit of Renewable Energy Development in Arid Zones (UDERZA), Univ. El-Oued, El Oued 39000, Algeria*
[d]*Centre National de Recherche en Sciences des Matériaux Tunisie*

0-20 wt % Cobalt doped hematite iron oxide (α-Fe_2O_3) thin films were deposited on 500°C heated glass substrates via spray pyrolysis method with moving nozzle. The dopant concentration is stepped as 0, 2%, 5%, 10%, and 20%. For the non doped thin film, XRD analyses exhibit the presence of diffraction peaks corresponding to planes (012), (104), (110), (113), (024), (116), (214), and (300) confirming the formation of α-Fe_2O_3 phase. While for the Co doped α-Fe_2O_3 thin films, further diffraction peaks corresponding to α-Fe_2O_3 phase, peaks matching well with the planes (200) and (311) of cobalt oxides CoO and Co_3O_4 respectively are observed. Co substitution was confirmed by XRD based on peaks shift of hematite towards higher angles. The crystallite size of the hematite increases from 37nm to 47nm with increasing dopant from 0 to 2wt. % Co/Fe. Then it decreases to 28nm for 20wt. % Co doping. While for cobalt oxides CoO and Co_3O_4, their crystallite sizes were found to be in the range of 29-32nm and 18-43nm, respectively.

The optical investigation indicates an increase in transmittance with increasing the dopant level reaching 80% at 600nm with blue shift in the band gap for the doped samples. FTIR study confirms the existence of the cobalt oxides at wave number average 460-542cm^{-1}. As an application in the areas of the antibacterial test, cobalt doped hematite nanoparticles (NPs) exhibit a good antibacterial activity against E. coli, Listeria innocua, Pseudo monas aeruginosa and Salmonella beyond 5wt. % Co/Fe doping.

(Received October 30, 2019; Accepted April 28, 2020)

Keywords: Co- α-Fe_2O_3, Spray pyrolysis, NPs, XRD, Antibacterial activity

1. Introduction

Iron is the fourth most abundant element in the crust of earth [1]. It exhibits as Fe (II) and Fe (III) in a variety of minerals including different types of iron oxides. The iron oxides are in fact oxides, hydroxides or oxihydroxides. All iron oxides and hydroxides are consisting of iron atom (Fe), oxygen atom (O) and hydrogen atom H or hydroxide OH group. They differ in coordination, in the valence of iron atom and, moreover, in the structure of crystal [2]. The different iron oxides have their own characteristics and qualities which are governed by the mineral structure. Iron oxides can be classified into sixteen mineral forms [3], The more important ones are: Goethite (α-FeOOH), Ferrihydrite ($Fe_5HO_8.4H_2O$), Akaganeite (β-FeOOH), Hematite (α-Fe_2O_3) Lepidocrocite (γ-FeOOH), Maghemite (γ-Fe_2O_3), Feroxyhyte (δ'-FeOOH), Magnetite (Fe_3O_4); most of these compounds are thermodynamically stable in natural systems (e.g. goethite, hematite, and magnetite) while others can be designated as intermediates only such as (ferrihydrite, maghemite) [1, 4-6]. The iron oxides have been developed in the form of nanopowders and thin films in order to employ them in wide variety areas of science and technology applications including medical use [7-9], environmental chemistry study [10-12], and soil treatment [13-15]. Also , industrial uses as

---

[*] Corresponding author: you.phy1988@gmail.com

pigment [16] and coating [17, 18] are taking part in those applications. Iron oxides nanomaterials synthesizing can be made through several methods, which can be generally classified as physical, chemical and biological manner [12]. To avoid the problems linked to the physical methods which suffered from the inability to control the size of particles in the nanometer range, spray pyrolysis is one of the efficient chemical methods utilized for such purpose, yet classical spray needs more than 1hour to elaborate one sample having as dimensions ($7.5x2.5x0.13cm^3$); In attempt to avoid this, spray with moving nozzle (SPMN) is used to avoid not only the spent time but also the heat drop of substrate during all the time of the samples elaboration. In order to improve the magnetic properties of hematite, various dopants have been used such as Ti [19], Al [20], Co [21], Cr [22]… etc. Among these dopants, cobalt with electronic configuration of [Ar] $3d^7 4s^2$ having one electron more than iron, has gained much attention. Cobalt atom gives one d and two s electrons to oxygen and keeps six electrons on its own atom. When Co is substituted for Fe with spin down electron, the spin down d band gets totally filled with one remaining spin up d-electron, This results in increasing in net magnetization in cobalt doped iron oxide [23].

There are some reliable reports in the literature that show encouraging results about the activity of different drugs and antimicrobial formulation in the form of NPs [24-26]. The biological activity of specific materials differs when the size of the constituting particles reduces to nanoscale dimension. An effective way to estimate the efficiency of NPs is to monitor the response bacteria exposed to these particles. Some antimicrobial gadgets are really toxic; thus why there is a big interest in finding ways to create new types of safe biocidal materials. Recently it has been confirmed that extremely reactive metal oxide nanoparticles show excellent evidence biocidal action against Gram-positive and Gram-negative bacteria [27].

Firstly, this work aims to deposit 0- 20 wt% cobalt doped hematite (α-Fe_2O_3) thin films on 500°C heated glass and anneal them for two hours at 550°C under atmosphere conditions [2]. The next is to study their structural and optical properties upon dopant concentration. Finally antimicrobial testing of Co-doped hematite NPs against Escherichia Coli, Listeria innocua, Pseudo monas aeruginosa and SaLMonelle will take place in this study.

2. Experimental details

2.1. Thin films preparation

Cobalt doped iron oxide NPs were prepared using SPMN method as described in Fig.1. To obtain mother solution of 0.5M of Fe^{+3}, 1.622g of iron chloride ($FeCl_3$) was dissolved in 20mL of distilled water and ethanol mixture in volume ratio 1:1 and stirred vigorously until complete dissolution (red brownish solution). Then, different quantities of cobalt chloride $CoCl_2$ were added to this solution with keep stirring for 30 min to get a range of dopant concentration (2, 5, 10, and 20 wt %). The obtained blends were sprayed onto 500°C heated glass substrates (Ref 217102: having $7.5x2.5x0.13cm^3$ as dimensions). The deposition time was 3min with spray rate of 5ml/min and kept distance nozzle-substrate of 5cm. Moving nozzle and high deposition temperature are used to preserve the stability of substrate and oxidation reaction temperatures. The prepared slides were annealed for two hours at 550°C.

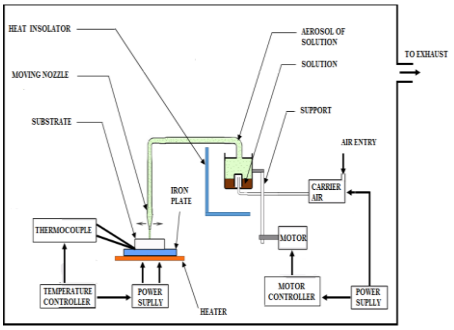

Fig. 1. Spray pyrolysis technique with moving nozzle (SPMN).

2.2. Thin films characterization

The crystallographic structure of 0-20 wt. % Co-doped α-Fe_2O_3 thin films have been examined via a Philips X-ray diffractometer model PW-1710 operating with ($\lambda = 1.5406$ Å for Cu-Kα radiation). Optical properties such as transmittance and band gaps have been undergone through the optical transmittance spectrum using (UV–VIS spectrophotometer Shimadzu, Model 1800) working in 300-900nm wavelength range. Whereas FT-IR analysis was performed, in 400-4000cm^{-1}range, by use of Shimadzu IR-Infinity 1 apparatus. All the measurements were carried out at room temperature (rt).

2.3. Antibacterial assay

The antibacterial activity of paper composites was determined by disk diffusion assay using:

- Gram-negative as: Escherichia Coli, (ATCC25922 : E.C), Pseudo monas aeruginosa, (ATCC 27853 : P.S) and SaLMonelle, (CIP 81-3 : SLM)
- Gram-positive as Listeria innocua, (CLIP 74915 : Lis)

Miller Hinton agar (MHA) was poured into a sterilized Petri dish and solidified within 10 min. E. C, Lis, P.S and SLM bacterial suspensions were uniformly inoculated on solidified agar gel. Sterile disks with 6mm in diameter were placed in different Co-hematite nanoparticles solutions which were obtained via grating the slides and dissolving the result powder in Dimethyl sulfoxide (DMSO) having the formula $(CH_3)_2SO$. The discs were then sited over the MHA plates and incubated for 24h at 37^{o}C. The antibacterial activities were compared by the diameter of the inhibition zone around each paper disk.

3. Results and discussions

3.1. Structural properties

The XRD patterns of 0-20 wt. % Co-doped hematite thin films are presented in Fig. 2. For non doped samples, the observed peaks at 2θ: 24.23°, 33.24°, 35.70°, 40.95°,49.54°,54.18°, 62.50°, and 64.17°correspond to lattice plane of (*012*), (*104*), (*110*), (*113*), (*024*), (*116*), (*214*) and (*300*), respectively confirm the formation of rhombohedral crystal structure of α-Fe_2O_3 and much well with its (JCPDS No: 01.073-2234, with space group R-3c number 167). For doped samples, all the observed peaks in the case of non doped samples persevere with approximately fixed slight shift to lower 2θ values for all Co dopant concentration. This shift may be due to the bigger radius of cobalt, compared to iron one ($R_{Co+2} = 0.72$Å, and $R_{Fe+3} = 0.64$ Å) [28].

For doping at 2 wt.%, a new peak appears in the XRD spectrum related to *(200)* plane, intensity of which fails down at 10 wt.% of doping; this peak corresponds to cobalt monoxide (CoO) reported to (JCPDS No: 01.043-1004). For doping much than 5 %, additional peak referred to *(311)* plane is observed and intensifies with mounting of doping. This indicates the presence of Cobalt (II, III) oxide (Co_3O_4) and much well with (JCPDS No: 01.065-3103). This is in good agreement with what showed in literature [29] and ensure that the used Co doping concentration (more than 2 wt. % Co/Fe) affect the Fe_2O_3 crystallographic structure thin films.

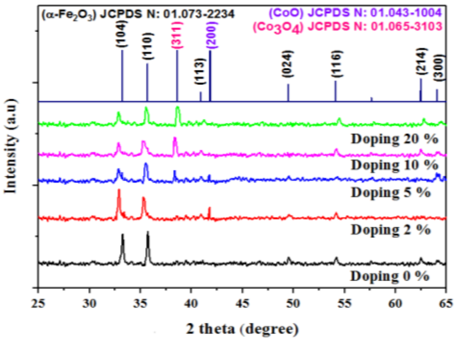

Fig. 2. X-ray diffraction patterns of sprayed hematite α-Fe_2O_3 of pure and Co-doped thin films.

The lattice constants (a and c), for the rhombohedral phase structure, are determined by the relations [9]:

$$2d_{hkl}\sin(\theta) = n\lambda \tag{1}$$

and

$$\frac{1}{d_{hkl}{}^2} = \frac{4}{3a^2}(h^2 + k^2 + hk) + \frac{l^2}{c^2} \tag{2}$$

where 'd_{hkl}'and (hkl) are the inter-planer distance and Miller indices, respectively. The values of lattice parameters 'a' and 'c' are listed in Table 1. It is worth noting that the values (a = b = 5.0272Å, c = 13.717Å) of the pure samples are close to the ones of the standard JCPDS data card, (a_0 =b_0 = 5.0325 Å and c_0 = 13.7404Å). Fig. 3 shows the lattice parameters (a and c) calculated from the XRD measurements as a function of the dopant concentration. The increase in lattice parameters of Co doped hematite thin films compared with the non doped one is due to the substitution of larger ionic radii of Co2+ into the position of smaller ionic radii of Fe^{3+} in α-Fe_2O_3 lattice. Those values are increased by very small amount up to 2wt.%, this confirms elongation of unit cell along c-direction hence Δc more than Δa. The constant values of lattice parameter after 2wt.% of cobalt doping may refer to that the substitution process of iron ions have been saturated.

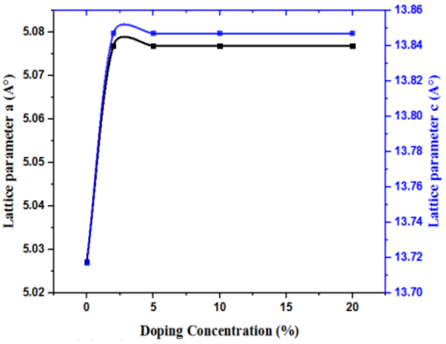

Fig. 3. Lattice parameter (a and c) of hematite α-Fe_2O_3 thin films upon Co doping concentrations.

Table 1. 0-20wt.% Co doped thin films parameters: d_{hkl},, average grain size, lattice parameters, optical gap, and Urbach energy.

Co/α-Fe_2O_3	hkl	2θ	FWHM$_β$ (Å)	D(nm)	d_{hkl}(Å)	Lattice parameters (Å)	Unit cell volume (Å^3)	Eu (eV)	Eg (eV)
0%	104	33.239	0.22367	37.08	d_{104}=2.6945	a=5.0272 c=13.717	300.212	0.217	2.07
	110	35.709	0.21831	38.24	d_{110}=2.5136				
2%	104	32.920	0.17457	47.46	d_{104}=2. 7199	a=5.0769 c=13.847	309.079	0.194	2.09
	110	35.348	0.24193	34.49	d_{110}=2.5384				
	200	41.697	0.26024	32.67	d_{200}=2.1654	a=4.3308			
5%	104	33.920	0.19125	43.32	d_{104}=2.7199	a=5.0769 c=13.847	309.079	0.160	2.12
	110	35.348	0.31256	26.70	d_{110}=2.5384				
	200	41.796	0.28784	29.55	d_{200}=2.1605	a=4.3210			
	311	38.310	0.19135	43.97	d_{311}=2.3487	a =7.7898			
	104	32.920	0.22826	36.30	d_{104}=2.7199	a=5.0769			

Co/α-Fe_2O_3	*hkl*	2θ	FWHM$_\beta$ (Å)	D(nm)	d_{hkl}(Å)	Lattice parameters (Å)	Unit cell volume (Å^3)	Eu (eV)	Eg (eV)
10%	**110**	**35.348**	**0.40925**	**20.39**	**d_{110}=2.5384**	**c=13.847**	**309.079**	**0.352**	**2.15**
	311	**38.310**	**0.39597**	**21.24**	**d_{311}=2.3487**	**a=7.7998**			
20%	**104**	**32.920**	**0.28934**	**28.63**	**d_{104}=2.7199**	**a=5.0769** **c=13.847**	**309.079**	**0.409**	**2.22**
	110	**35.348**	**0.35697**	**23.38**	**d_{110}=2.5384**				
	311	**38.300**	**0.46553**	**18.07**	**d_{311}=2.3493**	**a=7.7918**			

The crystalline sizes of 0-20wt.% Co doped thin films, given in Table.1, were calculated for the more intense peaks using Scherrer's formula[30] :

$$D = \frac{0.9\,\lambda}{\beta cos\theta} \tag{3}$$

where D, β, λ, and θ are the crystallite size, the full width at half-maximum (FWHM) of the considered diffraction peak, the X-ray wavelength (1.5406 Å) and Bragg angle, respectively. Shown in Fig. 4, is the Crystallite size variation; it increases from 37.08nm for undoped hematite nanoparticles to 47.46 nm for 2% doping. By increasing the dopant concentration to 5%, the crystallite size decreases to 43.32nm. For dopant concentration of 10%, crystallite size is reduced to 36.30nm, this value keeps decreasing to 28.63nm till 20% dopant concentration. Decrease in crystallite size at dopant concentration starting from 5% can be attributed to presence of cobalt ions which coincide with oxygen forming its own oxide (CoO and Co_3O_4), this can be defined as a crystal defects which well match with increasing in the urbache energy. The reduction in crystallite size was observed as a result of cobalt oxide presence in the films.

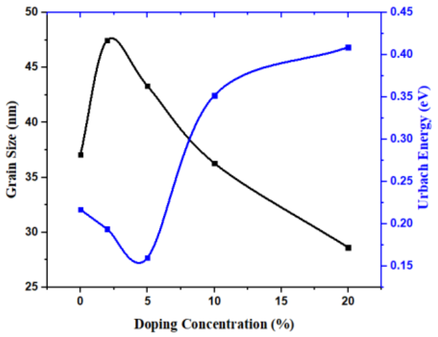

Fig. 4. Variation of Grain size and Urbach energy 0-20wt% Co doped thin films.

3. 2. Surface morphology

The surface morphology of Co doped iron oxide thin films (Co-α-Fe2O3) are studied via SEM. Fig. 5 (a,b,c, and d) shows the results with different doping concentration (2,5,10, and 20wt.%) respectively. The SEM images demonstrate that the grain size is homogeneous with some agglomerating sites. The average grain sizes are: 166,200,227, and 225 nm for 2,5,10, and 20wt.% respectively, those value are much higher than which were found in XRD, which confirm the fact that each grain is formed by aggregation of few numbers of nanocrystals.

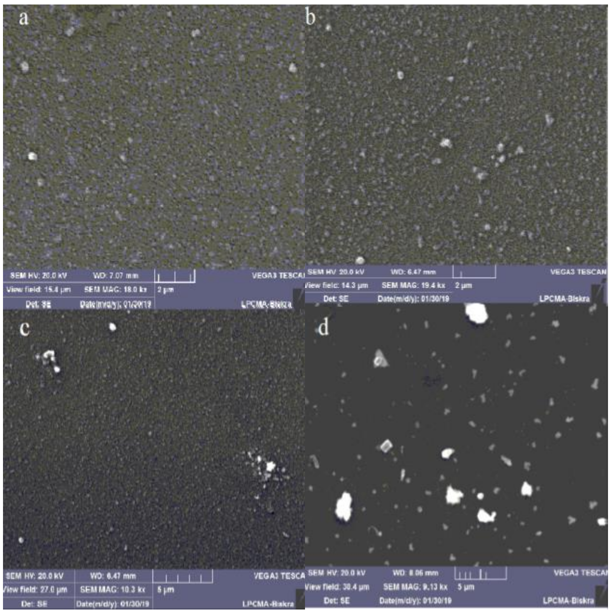

Fig. 5. SEM analysis of 0-20wt.% Co doped hematite thin films.

3.3. Optical properties

Photos of elaborated thin films are presented in Fig.6 which exhibits the change in color as a function of doping concentration. Fig. 7 shows the transmittance spectrum of 0-20wt.% Co doped thin films. For the undoped sample, the transmittance spectrum was found to be about 65% beyond 550nm. For the doped ones this value decreases to reach 60% at dopant concentration 2%, then increases to exceed 80% for the 5 and 10% wt Co doped samples whereas for 20 % Co doped sample the value of transmittance becomes lower than 80%. Bellow 550nm, the transmittance spectrum display a drastic decrease due the fundamental absorption of the materials (*i.e* the band gap).

The band gap has been calculated using, Tauc's relation as follow [31]:

$$\alpha h\nu = A(h\nu - E_g)^{\,n} \tag{4}$$

where α, h, ν, and E_g are the absorption parameter, Planck constant, the photon frequency, and gap energy, respectively; A is a constant and n is taken 2 based on the consideration that α-Fe_2O_3 has an indirect gap [32, 33]. The optical absorption data was used to plot $(\alpha h\nu)^2$ vs $h\nu$, as shown in Fig. 8, the straight line extrapolation leads to the band gap energy values of 0-20 wt .% Co doped samples. An obvious increase (blue shift) in Eg for the Co doped hematite thin films compared to the non doped ones; Eg increases from 2.07 for pure α-Fe_2O_3 to 2.09, 2.12, 2.15, and 2.22eV in respect to the dopant concentration 2%, 5%, 10%, and 20 wt.%, respectively. It is worth noting that the first ionization energy of Cobalt (7.88eV) is less than that one of iron (7.90eV) leading to a localization 3d orbital of cobalt higher than 3d orbital of iron This can causes an active transitions engaging 3d levels in Co^{+2} ions and strong pd-d exchange interaction between itinerant pd α-Fe_2O_3 orbits and the restricted d of the dopant. As a result a narrowing in the conduction band E_C and the valence band E_V happens and causes a shift of E_C upwards and E_V downwards, which leads to proclaim that Co doping causes the band gap broadening. The same phenomena (blue shift) are carried out in the literatures [[28], [31], [31]]

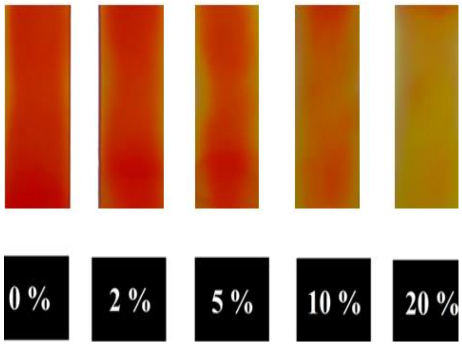

Fig. 6. Photographs of elaborated samples of 0-20% wt Co-doped α-Fe_2O_3 thin films.

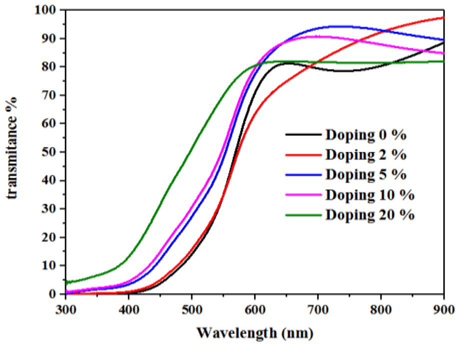

Fig. 7. Transparency spectrum of (0-20wt. %) Co-doped α-Fe_2O_3 thin films.

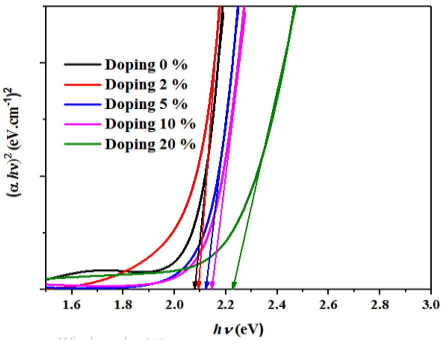

Fig. 8. Estimated band gap (E_g) from Tauc's relation for 0-20%wt Co doped α-Fe_2O_3 thin films.

3.4. FTIR

Fig. 9 shows the FTIR spectra of the Co-doped α-Fe_2O_3 thin films upon different dopant concentration. The peaks in the range 460-563cm^{-1} were attributed to the Fe-O and Co-O stretching mode [28]. The peaks intensity and the area absorption increase directly with the dopant concentration specifically at 20 wt. % (see inset), which gives rise in the compound formation of iron and cobalt oxides. The absorption peak centered at 1640 cm^{-1} indicates the presence of COO-stretch mode [17, 34]. While the absorption one at 2358 cm^{-1} is referred to the presence of CO_2 molecules, which may refer to the surrounding atmosphere during preparation.

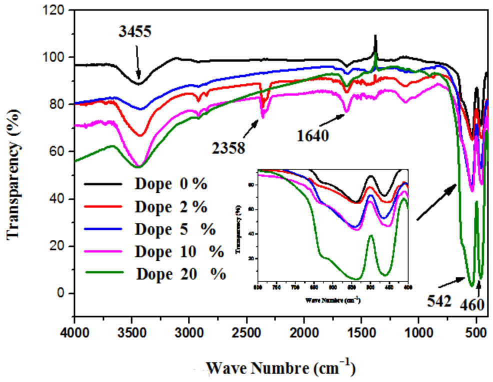

Fig. 9. FTIR spectrum of α-Fe_2O_3 of pure and Co-doped thin films.

3.5. Antibacterial activity

The antimicrobial activity of Co-hematite nanoparticles was given in Fig. 10. The nanoparticles correspond to 20% Co doping show an activity against E. coli and Lis. For 10% there are activity against P.a, SLM and Lis. For 5% of doping there are activity against E. coli and P. a. No activity was shown for 0% and 2%. From this study, it may be revealed that high doped Co-hematite nanoparticles exhibits good activity against both the gram positive and gram negative organisms.

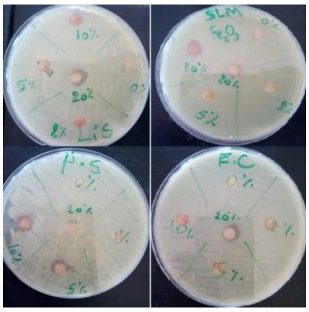

Fig. 10. Inhibitation Zone for different bacteria as a function of doping concentrations.

4. Conclusions

Cobalt doped iron oxide (hematite) nanoparticles were prepared using spray pyrolysis method. The dopant concentration is varied at 2, 5, 10, and 20wt.%. Presence of diffraction peaks corresponding to plans (*012*), (*104*), (*110*), (*113*), (*024*), (*116*), (*214*), and (*300*) signified the hematite phase formation. As a result of doping, two added peaks were appeared much well to planes (*200*) and (*311*) which correspond to cobalt oxides CoO and Co_3O_4 respectively. The peaks positions corresponding to hematite marked a fixed slight shift to lower 2θ values for all Co dopant concentration. Crystallite size increases in the beginning of dopping than it take a successive reduce values in increase at dopant concentration. The optical transmittance and the band gap values increase with increasing the dopant concentration. FTIR study confirms the existence of both Iron and Cobalt oxides. As an application in the areas of the antibacterial test, the synthesized cobalt doped hematite NPs exhibit a good antibacterial activity against E. coli, Listeria innocua, Pseudo monas aeruginosa and Salmonella beyond 5wt. % Co/Fe doping.

References

[1] J. L. Jambor, J. E. Dutrizac, Chemical Reviews **98**(7), 2549 (1998).

[2] Y. Meftah, D. Bekker, B. Benhaoua, A. Rahal, A. Benhaoua, A. Hamzaoui, Digest Journal of Nanomaterials and Biostructures, **13**(2), 465 (2018).

[3] R. M. Cornell, U. Schwertmann, The iron oxides: structure, properties, reactions, occurrences and uses, John Wiley & Sons, 2003.

[4] R. Cornel, U. Shwertmann, Iron oxides in the laboratory. Preparation and characterization, VCH Editions, Weinhein, Germany, 1991.

[5] V. Uwamariya, Adsorptive removal of heavy metals from groundwater by iron oxide based adsorbents, IHE Delft Institute for Water Education, 2013.

[6] H. Wigger, Environmental Release of and Exposure to Iron Oxide and Silver Nanoparticles: Prospective Estimations Based on Product Application Scenarios, Springer, 2017.

[7] R. V. Kumar, Y. Diamant, A. Gedanken, Chemistry of Materials **12**(8), 2301 (2000).

[8] R. Schrebler, K. Bello, F. Vera, P. Cury, E. Muñoz, R. del Río, H.G. Meier, R. Córdova, E. A. Dalchiele, Electrochemical and solid-state letters **9**(7), C110 (2006).

[9] G. Binitha, M. Soumya, A. A. Madhavan, P. Praveen, A. Balakrishnan, K. Subramanian, M. Reddy, S. V. Nair, A. S. Nair, N. Sivakumar, Journal of Materials Chemistry A **1**(38), 11698 (2013).

[10] K. Woo, J. Hong, S. Choi, H.-W. Lee, J.-P. Ahn, C. S. Kim, S. W. Lee, Chemistry of Materials **16**(14), 2814 (2004).

[11] A. Al-Hobaib, K. M. AL-Sheetan, L. El Mir, Materials Science in Semiconductor Processing **42**, 107 (2016).

[12] A. Ali, M. Z. Hira Zafar, I. ul Haq, A. R. Phull, J. S. Ali, A. Hussain, Nanotechnology, science and applications **9**, 49 (2016).

[13] D. Yokoyama, K. Namiki, H. Fukasawa, J. Miyazaki, K. Nomura, Y. Yamada, Journal of radioanalytical and nuclear chemistry **272**(3), 631 (2007).

[14] S. Laurent, D. Forge, M. Port, A. Roch, C. Robic, L. Vander Elst, R. N. Muller, Chemical reviews **108**(6), 2064 (2008).

[15] A. M. Jubb, H. C. Allen, ACS Applied Materials & Interfaces **2**(10), 2804 (2010).

[16] G. Zelmanov, R. Semiat, Water research **42**(1-2), 492 (2008).

[17] R. Todorovska, S. Groudeva-Zotova, D. Todorovsky, Materials Letters **56** (5), 770 (2002).

[18] S. Kulkarni, C. Lokhande, Materials chemistry and physics **82**(1), 151 (2003).

[19] X. Wang, K. Maeda, A. Thomas, K. Takanabe, G. Xin, J. M. Carlsson, K. Domen, M. Antonietti, Nature materials **8**(1), 76 (2009).

[20] D. B. Shinde, J. Debgupta, A. Kushwaha, M. Aslam, V. K. Pillai, Journal of the American Chemical Society **133**(12), 4168 (2011).

[21] M. Pelaez, N. T. Nolan, S. C. Pillai, M. K. Seery, P. Falaras, A. G. Kontos, P. S. Dunlop, J. W. Hamilton, J. A. Byrne, K. O'shea, Applied Catalysis B: Environmental **125**, 331 (2012).

[22] E. Yilmaz, C. Yogi, K. Yamanaka, T. Ohta, H. R. Byon, Nano letters **13**(10), 4679 (2013).

[23] A. Akbar, S. Riaz, R. Ashraf, S. Naseem, IEEE Transactions on Magnetics **50** (8), 1(2014).

[24] F. Forestier, P. Gerrier, C. Chaumanrd, A.-M. Quero, P. Couvreur, C. Labarre, Journal of Antimicrobial Chemotherapy **30**(2), 173 (1992).

[25] M. Fresta, G. Puglisi, G. Giammona, G. Cavallaro, N. Micali, P. M. Furneri, Journal of pharmaceutical sciences **84**(7), 895 (1995).

[26] V. P. Shah, K. K. Midha, J. W. Findlay, H. M. Hill, J. D. Hulse, I. J. McGilveray, G. McKay, K. J. Miller, R. N. Patnaik, M. L. Powell, Pharmaceutical research **17**(12), 1551 (2000).

[27] P. K. Stoimenov, R. L. Klinger, G. L. Marchin, K. J. Klabunde, Langmuir **18** (17), 6679 (2002).

[28] R. Satheesh, K. Vignesh, A. Suganthi, M. Rajarajan, Journal of Environmental Chemical Engineering **2**(4), 1956 (2014).

[29] S. Anjum, R. Tufail, K. Rashid, R. Zia, S. Riaz, Journal of Magnetism and Magnetic Materials **432**, 198 (2017).

[30] T. Mariño-Otero, M. Oliver-Tolentino, M. A. Aguilar-Frutis, G. Contreras-Martínez, E. Pérez-Cappe, E. Reguera, international Journal of Hydrogen Energy **40**(17), 5831 (2015).

[31] B. K. Ozcelik, C. Ergun, Ceramics International **41**(2), 1994 (2015).
[32] S. Shinde, R. Bansode, C. Bhosale, K. Rajpure, Journal of Semiconductors **32**(1), 013001 (2011).
[33] A. A. Yadav, T. Deshmukh, R. Deshmukh, D. Patil, U. Chavan, Thin Solid Films **616**, 351 (2016).
[34] C. Zhang, Z. Yu, G. Zeng, B. Huang, H. Dong, J. Huang, Z. Yang, J. Wei, L. Hu, Q. Zhang, Chemical Engineering Journal **284**, 247 (2016).